NRC Research Press

ARTICLE

# Case study of slope failure during construction of an open pit mine in Indonesia

Wei Wang and D.V. Griffiths



**Abstract:** This paper presents back-analyses of a failed slope at an open pit lignite mine in Muara Enim, Indonesia. The slope, which was being raised by the dumping of excavated material, failed at a dump height of 24 m, well before reaching the design height of 80 m. The primary cause of failure was determined to be the presence of a previously unknown weak layer in the foundation, combined with high excess pore pressures generated by a relatively fast dumping rate. The failure resulted in significant disruption of the mining operation, in addition to environmental problems and a high cost of remediation. Finite element analyses were performed to gain a better understanding of the influence of the weak layer at the time of the failure. The case history emphasizes the need for a thorough site investigation and the risks associated with fast dumping on saturated weak clay overlain by a stiff residual soil layer with low permeability.

*Key words:* slope stability, weak clay, excess pore-water pressure, undrained strength, finite element approach.

**Résumé :** Cet article présente des analyses rétrospectives d'une pente ratée dans une mine de lignite à ciel ouvert à Muara Enim, en Indonésie. La pente, qui a été soulevée par le déversement de matériaux excavés, a échoué à une hauteur de décharge de 24 m, bien avant d'atteindre la hauteur prévue de 80 m. La principale cause d'échec a été déterminée par la présence d'une couche faible jusque-là inconnue dans la fondation, combinée à des pressions interstitielles élevées générées par un taux de décharge relativement rapide. La rupture a entraîné une perturbation importante de l'exploitation minière, en plus des problèmes environnementaux et des coûts élevés d'assainissement. Des analyses par éléments finis ont été effectuées pour mieux comprendre l'influence de la couche faible au moment de la rupture. L'historique du cas met l'accent sur la nécessité d'une étude approfondie du site et sur les risques associés à un déversement rapide sur de l'argile faible saturée, recouverte par une couche de sol résiduel rigide et faiblement perméable. [Traduit par la Rédaction]

*Mots-clés :* stabilité des pentes, argile faible, excès de pression de l'eau interstitielle, force non drainée, approche par éléments finis.

## Introduction

With increasing adoption of surface mining of coal, problems associated with waste dump instability — which affects resource recovery, mining cost, and safety, and presents environmental hazards — have become a matter of prime concern to mine planners and operators. There exist many examples of waste dump instabilities worldwide, with a considerable bibliography (e.g., Richards et al. 1981; Okagbue 1986; Ulusay et al. 1995; Dawson et al. 1998; Steiakakis et al. 2009). These large-scale failures and their negative consequences have focused the attention of numerous researchers on the importance of stability during waste dumping in open pit mining.

Mining waste is often dumped in mountainous terrain; however, the handling and disposal of mining waste heaped on near-horizontal ground is also common, and is comparable in magnitude and potential modes of failure to that involved in earth-moving operations for dams, road and railway embankments, and other civil engineering operations. This paper presents back-analyses of a failed waste dump slope heaped on near-horizontal ground at an open pit mine in Muara Enim, Indonesia. A mechanism of foundation failure of fills by spreading during construction has been studied in this paper, and is known to occur in connection with fills located above stratified deposits that contain layers of soft clay (e.g., Cooling and Golder 1942; Terzaghi et al. 1996). Failure mechanisms can vary widely depending on the geological, groundwater, and drainage conditions. Failure by spreading with partial to negligible consolidation of weak foundations during staged construction have been of interest to many researchers (e.g., Ladd 1991; Duncan and Wright 2005). In all cases, estimation of the distribution and generation of pore-water pressure during undrained loading is of crucial importance. In this paper, a new approach combining finite element (FE) stability analyses by "strength reduction" with coupled analysis to predict pore-water pressure response to undrained loading was adopted to simulate the failure during continuous construction. The aim of this paper is to improve understanding of failure mechanisms and serve as a useful reference for similar projects.

### Background

The Muara Enim Mine (MEM) is one of the currently active open pit mines in South Sumatra, Indonesia. It is located in the Dangku region, 100 km southwest of Palembang, 10 km west of Prabumulih (Fig. 1), and is operated by the China Shenhua Group Corporation (CSGC).

Received 16 November 2017. Accepted 5 July 2018.

**W. Wang.** State Key Laboratory of Geohazard Prevention and Geoenvironment Protection; Chengdu University of Technology, Chengdu 610059, China.
**D.V. Griffiths.** Colorado School of Mines, 1500 Illinois Street, Golden, CO 80401, USA; Centre for Geotechnical Science and Engineering (CGSE), The University of Newcastle, Callaghan, NSW 2308, Australia.
**Corresponding author:** Wei Wang (email: wwei@cdut.edu.cn).



 Published at www.nrcresearchpress.com/cgj on 31 July 2018.

**Fig. 1.** East dumping site plan sketch and investigation plan. DCPT, dynamic cone penetration test. [Colour online.]

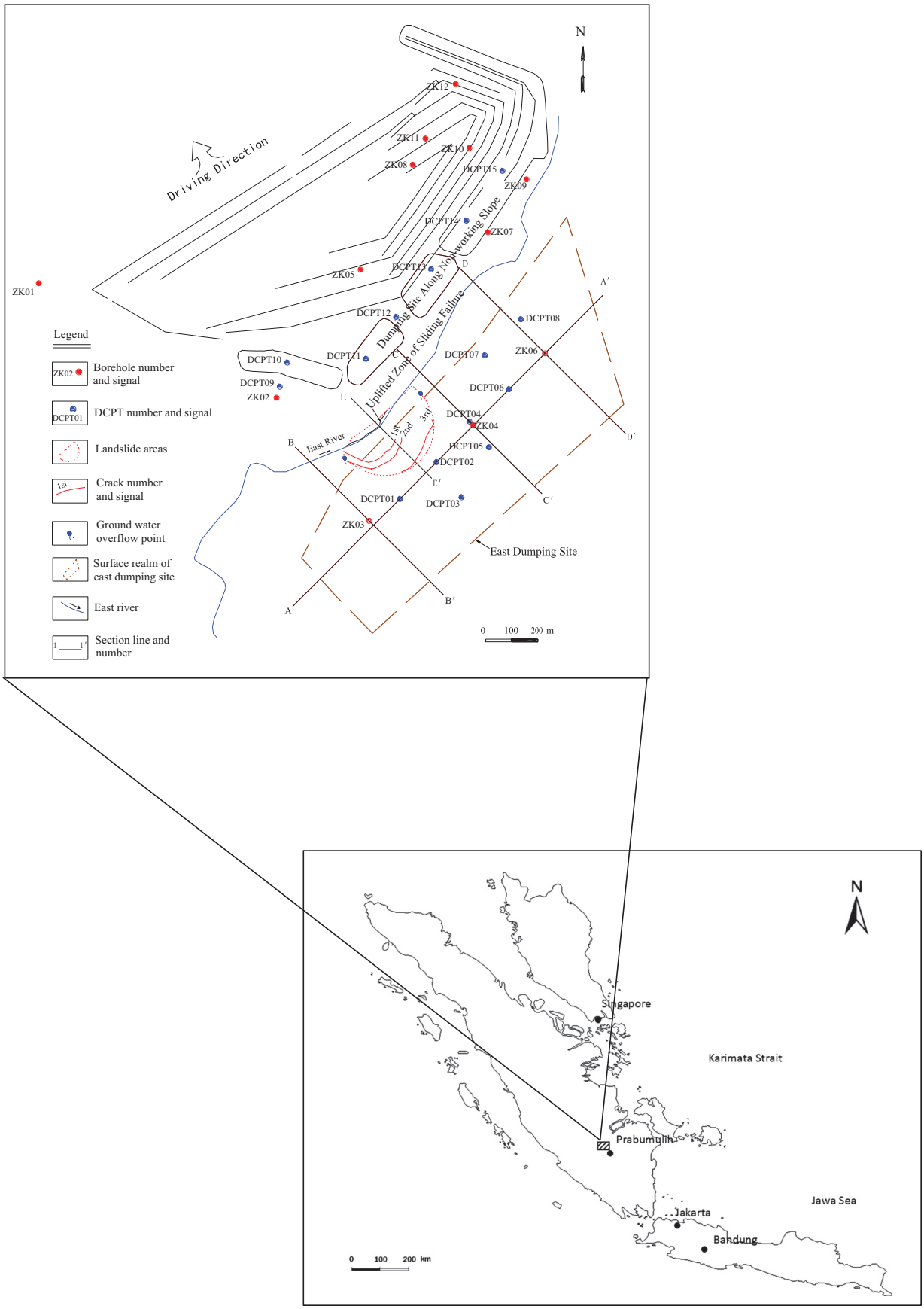

**Fig. 2.** C–C′ schematic geological section and design of dumping slope.

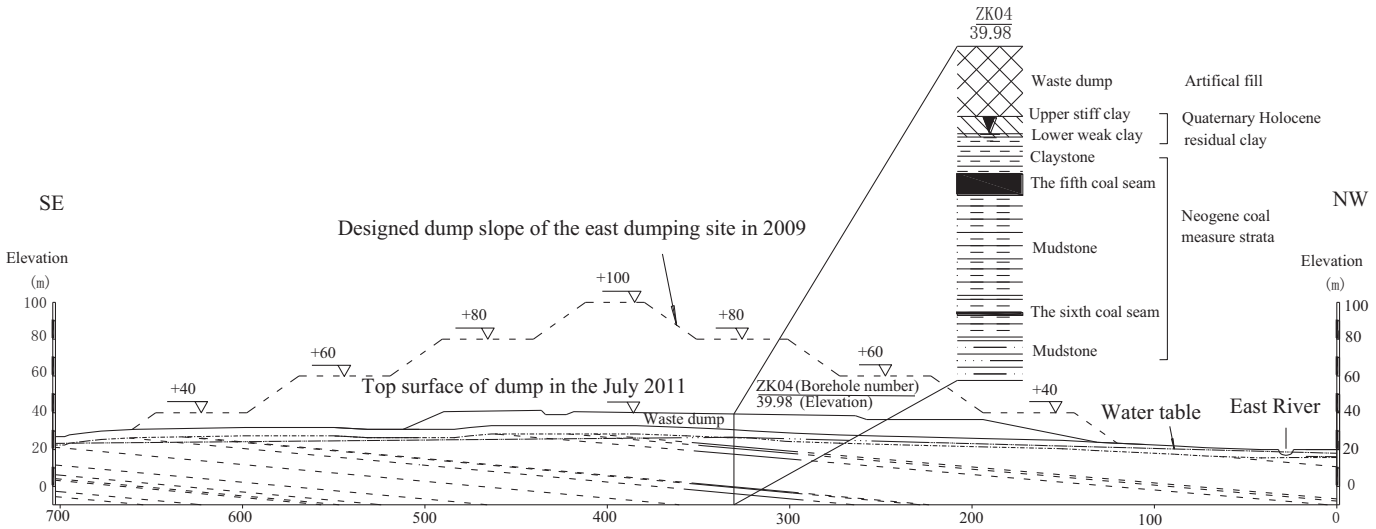


The MEM has been estimated to contain 71.06 Mt of coal reserves, which will provide a service life of 30 years for the local power plant. Construction of the MEM started at the end of 2009 and operations commenced in 2010, using a discontinuous mining method that employs single-bucket excavators, heavy trucks, and bulldozers.

Construction of the mine involved excavated material that was dumped using trucks. The east dumping site, which was the first put into use, covered a plan area of approximately 1500 m by 540 m, with a dumping capacity of 39 $Mm^3$ (Fig. 1). The total dump height in the original design was 80 m, divided into four benches, each with a height of 20 m, a width of 50 m, and an overall dump slope inclination of 3.1:1.

On 28 June 2012, when the east dump slope reached a height of 24 m, a failure initiated on the northwest side of the dump slope. In the initial month of the failure, cracks developed from the first bench to the second, in the form of a retrogressive failure. The instability involved the mobilization of a mass of 1.7 $Mm^3$, with an approximate width and length of 380 m by 195 m, respectively. The moving mass slid into the East River and blocked it, which resulted in significant disruption of the mining operation, in addition to environmental problems and a high cost of remediation. Because of the failure, the dump site was finally abandoned well short of its design height of 80 m.

The subsequent investigation indicated that the waste dump was founded on clay, which, as it was later discovered, contained a weak layer in the lower portion underlain by claystone and mudstone (Fig. 2).

## Description of the failure

The failure started on 28 June 2012 while the dump slope was being raised to a height of 24 m. Arc-shaped cracks (first and second) were observed at the crest of the first level bench, as well as water outlet points on the left and right flanks (Fig. 1). The mass between the two cracks slumped to form a trough-like depression (Figs. 1, 3, and 4). On 26 July 2012, a new crack (third) appeared on the second level bench (Figs. 1 and 4). A continuous uplift zone was also observed, approximately 3 m high, blocking the East River at the front edge of the landslide (Figs. 1, 4, and 5).

Sliding occurred perpendicular to the East River bank, which offered an unrestrained boundary. Field observations revealed that vertical movement occurred from the crest to the toe of the slope (Figs. 3, 6, and 7), and horizontal movement was observed at the toe of the slope towards the East River bank (Fig. 5), with a sliding distance estimated to be approximately 20 m.

**Fig. 3.** Photo of failure by spreading of first level bench. [Colour online.]


When the three cracks appeared, a total of six monitoring points were installed on the crest of the first and the second level bench (three monitoring points per bench). Displacement monitoring indicated that the mass between the first and second cracks on the first bench subsided approximately 2.5 m over a length of approximately 180 m between 28 June and 22 September 2012 (Fig. 6) and the slump of the mass between second and third cracks was about 4.4 m over a length of approximately 240 m between 26 July and 8 September 2012 (Fig. 7).

## History of geotechnical investigation and design of dump slope

Geotechnical investigations of the MEM dump slope went through three stages as follows:

### First stage

The design and the first stability analysis of the MEM dump slope were commenced in 2009 before construction. The strength parameters of the waste dump material, clay, claystone, and mudstone used in the analyses are shown in Table 1 (NSDI 2009; SYDRI 2009*a*). The parameters of the waste dump material and clay were determined from sites with similar engineering property values, and the parameters of the claystone and mudstone were estimated based on relatively few samples. The lower weak clay layer was not identified at this stage, therefore no parameters for this

**Fig. 4.** E–E′ schematic section showing geological structure, indicating thin weak clay stratum, drainage boundary, and real range of base of waste failure by spreading (units in metres, showing geometry at failure state in July 2012).

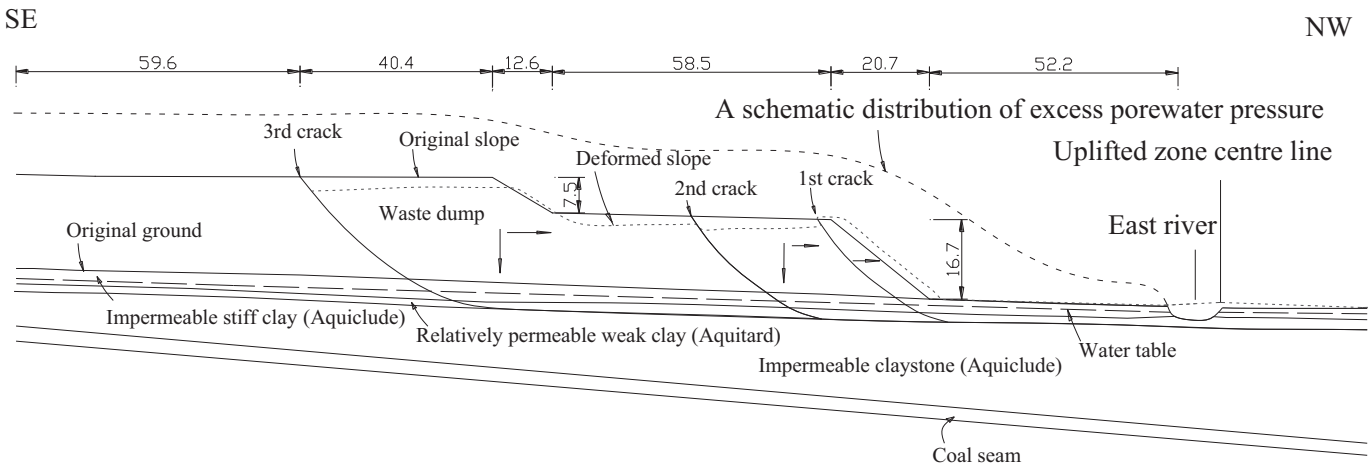


**Fig. 5.** A continuous uplift zone and bulging cracks on landslide toe. [Colour online.]


**Fig. 6.** Vertical movement between 28 June and 22 September 2012 of a monitoring point on crest of first level bench.

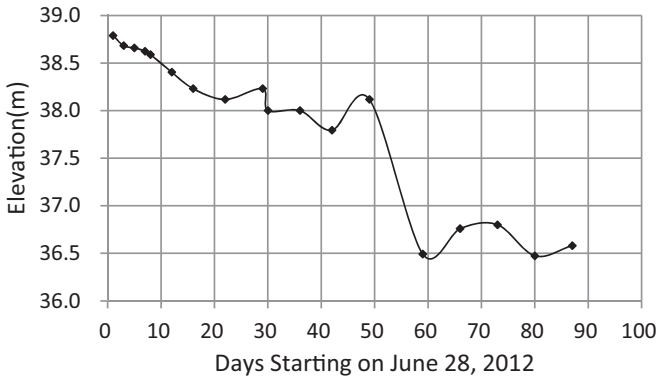


layer are shown in Table 1. The parameters of the clay were listed as that of upper stiff clay for comparison with those from 2011.

The total dump height of the original design was 80 m, divided into four benches, each with a height of 20 m, width of 50 m, and overall dump slope inclination of 3.1:1 (Fig. 2). The design geometry gave the final profile of the dump slope; however, actual

**Fig. 7.** Vertical movement between 26 July and 22 September 2012 of a monitoring point on crest of second level bench.

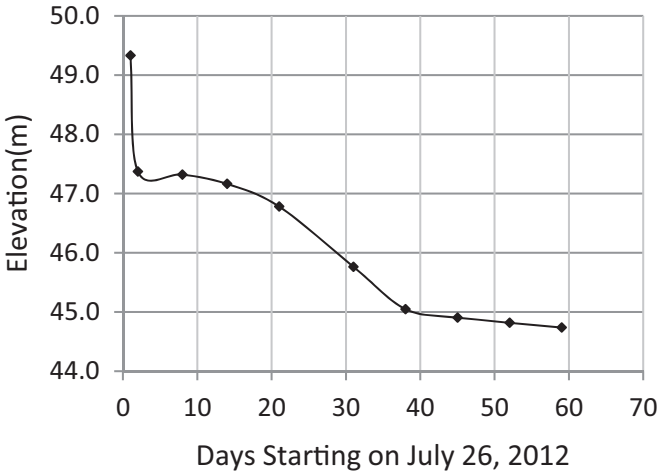


**Table 1.** Parameter values for slope stability analysis in 2009 and 2011.

| | | | Clay | | | | | | | |
|---|---|---|---|---|---|---|---|---|---|---|
| | Waste | | Upper stiff clay | | Lower weak clay | | Claystone | | Mudstone | |
| Parameter | 2009 | 2011 | 2009 | 2011 | 2009 | 2011 | 2009 | 2011 | 2009 | 2011 |
| $\gamma$ (kN/m³) | 18.6 | 16.5 | 18.6 | 17.8 | — | 17.8 | 16.7 | 15.5 | 15.9 | 15.9 |
| $c$ (kPa) | 20.0 | 10 | 20.0 | 50.0 | — | 15.0 | 30.0 | 80.0 | 100.0 | 110.0 |
| $\phi$ (°) | 20.0 | 17.5 | 22.0 | 20.0 | — | 13.0 | 21.5 | 22.0 | 23.8 | 23.0 |

dumping was conducted simultaneously on more than one bench. Based on the design geometry and properties, a factor of safety of 1.29 was computed by the methods based on circular sliding modes (SYDRI 2009*b*).

## Second stage

From April to December 2011, a specialized exploration and investigation was carried out by the project group at Chengdu University of Technology (PCUT) on the dump slope, which had reached a height of approximately 10 m. The investigation included 12 boreholes for standard penetration tests (SPTs) and 15 locations for dynamic cone penetration tests (DCPTs) (Fig. 1).

The strength parameters used in those analyses are also shown in Table 1 (PCUT 2011). The values of the waste dump material were

**Table 2.** Physical and mechanical properties of upper stiff clay and lower weak clay.

| Sample number | USCS[a] | Soil name | $G_s$ | $\gamma$ (kN/m$^3$) | $w$ (%) | Atterberg limits | | | $e$ | $S_r$ (%) | Direct shear | | | | Triaxial | | | |
|---|---|---|---|---|---|---|---|---|---|---|---|---|---|---|---|---|---|---|
| | | | | | | | | | | | Undisturbed | | Disturbed | | UU | | CU | |
| | | | | | | $w_l$ (%) | $w_p$ (%) | $I_p$ (%) | | | $c$ (kPa) | $\phi$ (°) | $c$ (kPa) | $\phi$ (°) | $c$ (kPa) | $\phi$ (°) | $c'$ (kPa) | $\phi'$ (°) |
| 9-ZK02-1 | CH | Fat clay[b] | 2.62 | 17.5 | 38.6 | 94.5 | 31.9 | 62.6 | 1.08 | 94 | — | — | 14 | 13.8 | — | — | — | — |
| 9-ZK04-1 | CH | Sandy fat clay[b] | 2.66 | 18.6 | 32.5 | 72.5 | 27.5 | 45.1 | 0.9 | 96 | — | — | — | — | — | — | — | — |
| 9-ZK10-1 | CH | Fat clay[b] | 2.6 | 16.7 | 44.3 | 74.5 | 29.5 | 45.0 | 1.24 | 93 | 37 | 22.1 | — | — | 57 | 17.4 | 12 | 34.7 |
| 9-ZK11-1 | CH | Fat clay[b] | 2.68 | 16.9 | 46.8 | 69.5 | 26.9 | 42.6 | 1.33 | 94 | 42 | 22 | 43 | 16.8 | 38 | 12 | 27 | 26.2 |
| 9-ZK12-1 | CH | Fat clay with sand[b] | 2.65 | 16.9 | 44.6 | 71 | 29.9 | 41.1 | 1.26 | 93 | 36 | 21.3 | — | — | — | — | — | — |
| 9-ZK09-1 | CL | Sandy lean clay[c] | 2.66 | 19.2 | 26.5 | 41.4 | 17.6 | 23.8 | 0.75 | 94 | 17 | 18.9 | 14 | 13.8 | — | — | — | — |

[a]Unified Soil Classification System (ASTM 2011b).
[b]Upper stiff clay.
[c]Lower weak clay.

**Table 3.** Parameter values for slope stability analysis.

| Parameter | Waste | Upper stiff clay | Lower weak clay | Bedrock |
|---|---|---|---|---|
| $\gamma$ (kN/m$^3$) | 16.5 | 17.3 | 19.2 | 16.8 |
| $c$ (kPa) | 10.0 | 36.9 | | 90.0 |
| $\phi$ (°) | 23.5 | 20.3 | | 20.0 |
| $c_u$ (kPa) | — | — | 18.3~45.3;[a] 2.7~13.9[b] | — |
| $E$ (kPa) | 8000 | 20 000 | 2000 | 25 000 |
| $\nu$ | 0.3 | 0.25 | 0.35 | 0.25 |
| Permeability (m/day) | — | — | 0.02 | — |

[a]Undrained peak strength at first stage when FOS was equal to unity.
[b]Undrained residual strength at failure stage when mechanism most similar to that observed in the field occurred.

**Fig. 8.** Groundwater outflow in weak layer discharged into exploratory trench. [Colour online.]

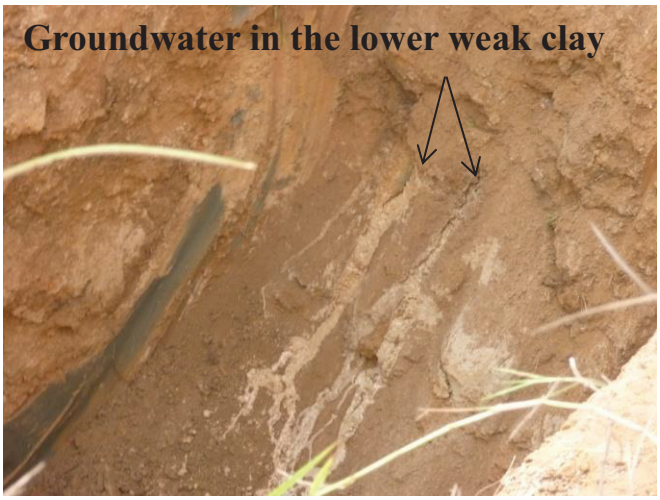


**Fig. 9.** Interlayer water seeping out of aquifers on excavated nonworking slope of mining field. [Colour online.]

obtained by back-analysis of a neighbouring small-scale dump slope where failure developed in the waste materials. The shear strength of the upper stiff clay, claystone, and mudstone were determined from laboratory direct shear tests shown later (see section titled "In situ and laboratory testing") with reference to soils with similar engineering property values. Samples were taken from boreholes, drilled at the research site.

**Fig. 10.** DCPT blow count vs. depth histogram: (*a*) DCPT01; (*b*) DCPT03; (*c*) DCPT04; (*d*) DCPT05.

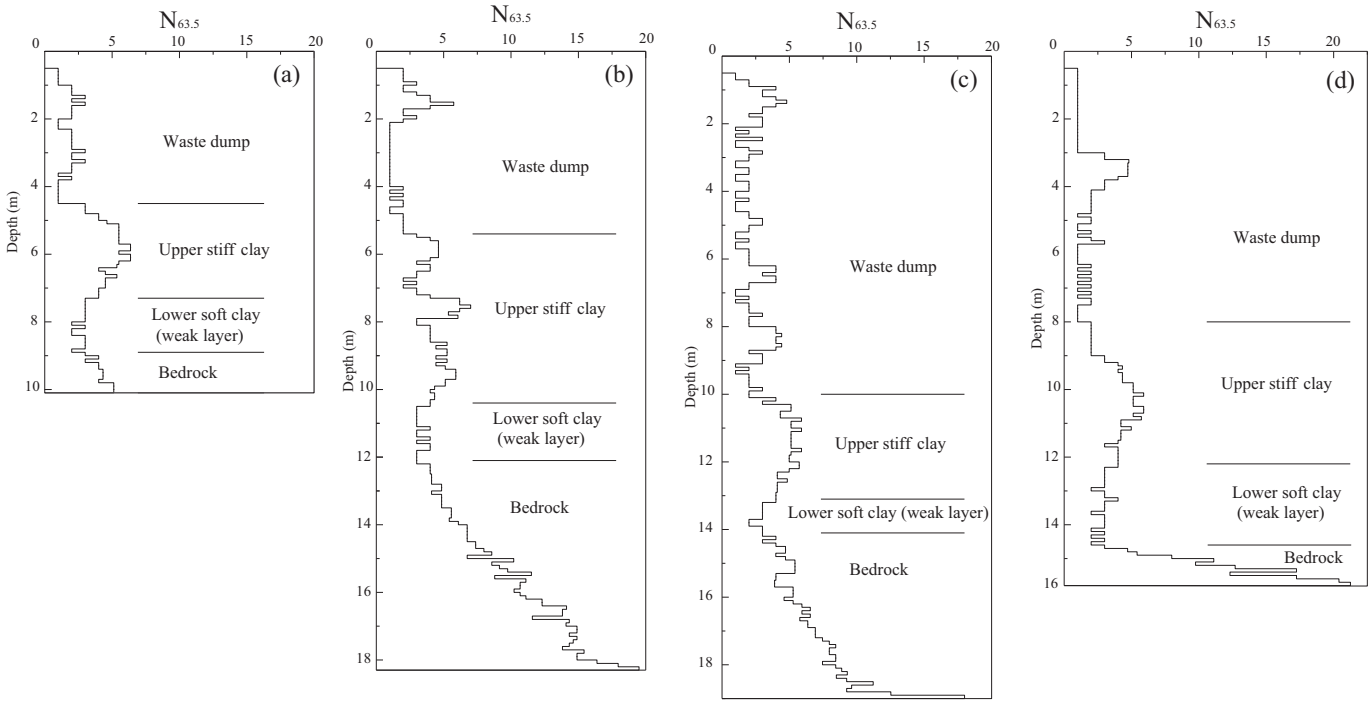


**Table 4.** SPT *N* blow count.

| | *N* (blows/30 cm) | | | | | |
|---|---|---|---|---|---|---|
| Soil type | ZK03 | ZK04 | ZK06 | ZK11 | ZK12 | Representative value |
| Waste dump | — | 3–8 | — | — | — | 8 |
| Upper stiff clay | — | 10 | — | 9 | 11–12 | 10 |
| Lower weak clay | 3 | — | 4 | — | 6–8 | 3–4 |

**Table 5.** Relation of consistency of clay, number of blows $N_{60}$ on sampling spoon, and unconfined compressive strength (data from table 12.2 in Terzaghi et al. 1996).

| $N_{60}$ | <2 | 2∼4 | 4∼8 | 8∼15 | 15∼30 | >30 |
|---|---|---|---|---|---|---|
| Consistency | Very soft | Soft | Medium | Stiff | Very stiff | Hard |
| $q_u$ (kPa) | <25 | 25∼50 | 50∼100 | 100∼200 | 200∼400 | >400 |

The lower weak clay was identified on site, but due to the difficulties in sampling undisturbed specimens and an incomplete understanding of the soil profile, sampling was insufficient and only a set of direct shear tests were performed with results shown in Table 2. These values were not considered very reliable parameters for use in a stability analysis. Consequently, the parameter values were determined from engineering experience as shown in Table 1, and the influence of excess pore-water pressure caused by undrained loading on the stability analyses was not considered at that time.

On the basis of the design geometry and the above parameter values, a factor of safety of 1.36 was computed by the methods of Morgenstern–Price (Morgenstern and Price 1965) using SLOPE/W. The potential slide surface developed in the waste dump material and along the interface between waste and the basal clay.

According to the latest research results presented in this paper and shown in Table 3, it is noted that the strength values of the waste dump were underestimated, and those of the upper stiff clay and lower weak clay were overestimated, leading to prediction of the wrong critical slip surface. The actual slip surface was highly translational and headed towards the river.

**Third stage**

After the failure occurred in 2012, the PCUT re-examined the failure mechanism and the stability analyses of the dump slope based on the data from 2011 as presented in this paper.

To determine the influence of the weak layer on the failure of the dump slope, two exploratory trenches were dug between the East River and the toe of the slope in July 2012. Figure 8 shows that the weak layer displayed an outflow of significant quantities of groundwater due to high water pressures. This observation provided important evidence to guide the assumptions used in the stability analyses presented later in this paper.

## Geology and hydrogeology of the area

The foundation of the east dumping site consists of Quaternary Holocene residual clay and Neogene coal measure strata. The residual clay of weathered rock material was in unconformable contact with the underlying coal measure strata of the Muara Enim Formation and divided into an upper stiff clay and a lower weak clay as described later. The thickness of the residual clay was approximately 1–5 m (Fig. 2). The coal measure strata consisted of

**Table 6.** Physical and mechanical properties of claystone and mudstone.

| Rock type | $G_s$ | $\gamma$ (kN/m³) | $\gamma_d$ (kN/m³) | $w$ (%) | Water absorption (%) | $e$ | $S_r$ (%) | Number of sets of tests: Undisturbed direct shear | Number of sets of tests: Triaxial UU |
|---|---|---|---|---|---|---|---|---|---|
| Claystone | 2.56 | 15.8 | 10.0 | 59.0 | 62.5 | 1.6 | 94.5 | 4 | 3 |
| Mudstone | 2.58 | 16.9 | 11.8 | 43.95 | 47.0 | 1.22 | 93.7 | 16 | 12 |

**Fig. 11.** Linear least-squares regression of undisturbed direct shear: (*a*) upper stiff clay; (*b*) claystone; (*c*) mudstone. [Colour online.]

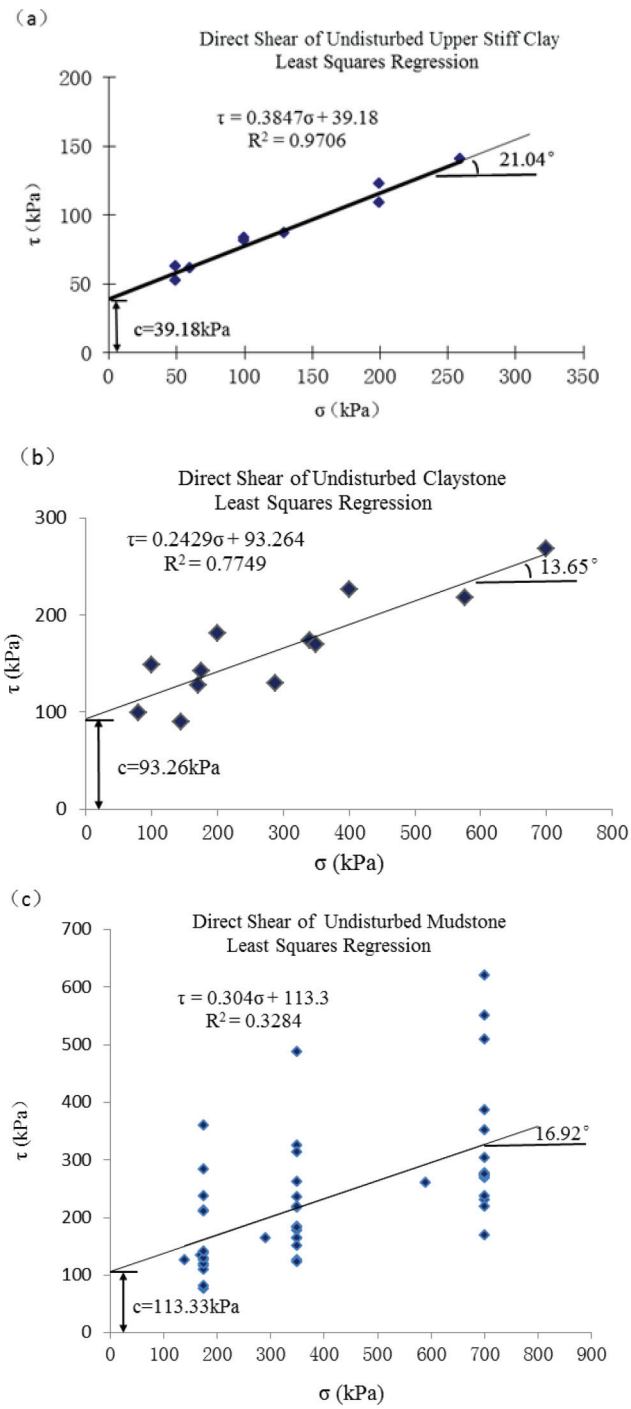


**Table 7.** Statistics estimated by the least squares and statistical method from undisturbed undrained direct shear strength tests of relative soil and rock.

| Statistical parameter | Soil and rock: Upper stiff clay | Claystone | Mudstone |
|---|---|---|---|
| Statistical sets/points | 3/9 | 4/12 | 16/48 |
| **Cohesion** | | | |
| Mean (kPa) | 39.18 | 93.26 | 113.33 |
| SD (kPa) | 3.71 | 14.34 | 27.55 |
| COV | 0.09 | 0.15 | 0.24 |
| CF | 0.94 | 0.92 | 0.94 |
| SV (kPa) | 36.86 | 85.74 | 106.71 |
| **Friction angle** | | | |
| Mean (°) | 21.04 | 13.66 | 16.92 |
| SD (°) | 1.26 | 2.24 | 3.24 |
| COV | 0.06 | 0.16 | 0.19 |
| CF | 0.96 | 0.91 | 0.95 |
| SV (°) | 20.25 | 12.49 | 16.14 |

claystone, mudstone, silty mudstone, pelitic siltstone, siltstone, fine sandstone, carbonaceous mudstone, and seam (NSDI 2009). No faults were observed, with a rock dip toward approximately N6°E and an inclination of 4°–6°.

With regard to hydrogeology, the lower clay, sandstone, silty mudstone, pelitic siltstone, and siltstone are water-bearing formations. The upper clay, claystone, and mudstone constitute water resisting layers (NSDI 2009; PCUT 2011). It was observed that interlayer water seeped out of aquifers on excavated nonworking slopes of the mining field as shown in Fig. 9. Therefore, groundwater supply and drainage were dominated by lateral runoff. Fluctuating phreatic surfaces developing in Quaternary residual clay made the whole site vulnerable to the development of high water pressures (Figs. 2 and 4), due to subsurface erosion leading to the bottom residual clay — namely, the lower weak clay — to later be sandy and have a higher permeability.

In addition, the East River is located between the mining field and the east dumping site and runs across the area from southwest to northeast (Fig. 1). The proximity of the river bank to the waste dump slope provided an unrestrained boundary surface for the waste dump to slide.

## Investigation of waste dump slope stability

The testing and investigation were concentrated on the waste dump, upper stiff clay, lower weak clay, and underlying bedrock composed of claystone and mudstone, which all had an influence on the stability of the slope. Re-analysis of the in situ and laboratory testing data as presented in this paper provides new insight into the soil engineering properties critical to a better understanding of the failure mechanism.

### In situ and laboratory testing

Drilling, in combination with SPTs and DCPTs, was adopted for the exploration and in situ testing. Three of the 12 boreholes (ZK03, ZK04, and ZK06) and eight of the 15 DCPT holes (DCPT01–DCPT08) were arranged at the east dumping site. With the exception of the DCPTs, all in situ and the following laboratory testing

**Fig. 12.** Model of in situ analysis (yellow: upper stiff clay; red: lower weak clay; green: bedrock; blue dotted line: water table; units in metres). [Colour online.]

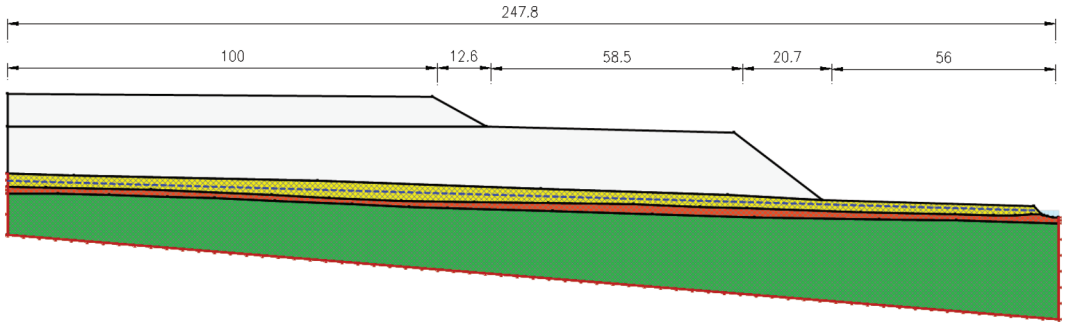


conformed to current ASTM standards (D1586-11 (ASTM 2011*a*) and D2487-11 (ASTM 2011*b*)).

The DCPT is gaining popularity as one of the most common field testing methods. Perhaps its most important advantage is the ability to provide a continuous record of soil strength with depth. It is fast, inexpensive, and particularly useful in delineating areas of weak soils overlying stronger strata and in quickly assessing the variability of soil conditions (Rowe 2001). In general, a heavy DCPT is suited to sand, granular soil, and soft rock. In this investigation, the drop weight was 63.5 kg with a drop distance of 76 cm.

The representative results from DCPT01, DCPT03, DCPT04, and DCPT05 are shown in Fig. 10, with corrected values using the formula

$$N_{63.5} = \alpha_1 N'_{63.5} \quad (1)$$

where the correction coefficient $\alpha_1$ is taken from the *Code for investigation of geotechnical engineering* (GB50021–2001), National Standard of the People's Republic of China (Ministry of Construction of the People's Republic of China 2009).

DCPT results indicated that an essentially continuous layer of the weak clay layer existed in the lower portion of the residual clay (Fig. 10). In summary, the clay layer can be divided into two sublayers as follows:

- The upper clay sublayer generally contained a surface organic clay layer 0.6~1.5 m thick overlying an intermediate clay layer, total thickness in the range of 1.2~4.0 m. To avoid the adverse effect, the organic clay layer was eliminated before construction. From representative SPT blow counts of the layer shown in Table 4, the consistency could be determined as "stiff" (Table 5). The sublayer was referred to as the upper stiff clay.
- The lower clay sublayer had a thickness varying in the range of 0.5~1.9 m, 1.2~4.0 m below ground. The consistency of the layer could be determined as "soft" from Tables 4 and 5. The sublayer was known as the lower weak clay.

  Also from Table 5, the undrained shear resistance of the lower weak clay could be estimated from the unconfined compressive strength to be in the range of 18.75~25 kPa.

Laboratory tests were conducted on surface clay and underlying bedrock from samples removed from boreholes, including analysis of mineralogical composition, Atterberg limits, grain size analysis, and shear strength.

Table 2 presents the specific gravity, unit weight, water content, liquid limit, plastic limit, plasticity index, void ratio, and degree of saturation of the upper stiff and the lower weak clays. It indicates that both layers were saturated, but the lower weak clay had a higher unit weight and lower water content, plasticity, and void ratio than the upper stiff clay. Consolidation tests performed on the upper stiff clay indicated that it was overconsolidated, with an overconsolidation ratio in the range of 5.8~14.5. The variation in

**Fig. 13.** Comparison of distribution of tvertical effective stress $\sigma'_{vo}$ for coefficients of permeability of 0.002, 0.02, and 0.2 m/day over undrained weak layer at time of failure.

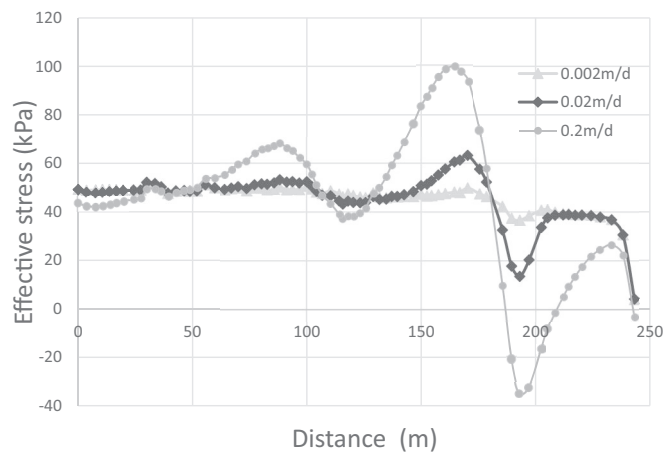


strength of the upper stiff and the lower weak clays involved not only the physical properties, but also the effect of groundwater and the initial stress state. Fluctuations of the groundwater level in the surface residual clay could have a significant influence on the reduction in strength of the lower weak clay (Terzaghi et al. 1996, p. 371; Jiao et al. 2005).

The physical properties of the saturated claystone and mudstone are shown in Table 6 indicating that they had a higher void ratio, water content, and lower unit weight than the clay (Table 2).

From water storage characteristics and hydraulic conductivity characteristics, the upper stiff clay, claystone, and mudstone could be thought of as an aquiclude, and the lower weak clay could be thought as an aquitard.

In 2011, triaxial (unconsolidated undrained, UU; consolidated undrained, CU) and direct shear tests were conducted to obtain undrained strength properties of the upper stiff clay, claystone, and mudstone shown in Tables 2 and 6, as shown in Fig. 11. Due to variability of specimen quality and the relatively few UU and CU tests performed, the results from direct shear tests were considered more credible. The rate of displacement for direct shear tests was 0.5 mm/min, which means strength properties obtained were under approximately undrained conditions.

By means of a linear least-squares regression analysis (Fig. 11), the mean and standard deviation of both the cohesion and friction angle of the upper stiff clay, claystone, and mudstone were obtained, shown in Table 7. These statistical values were used for determining the "best-fit" peak strengths of these three materials to be used later. In addition, the shear strength of lower weak clay, which was operating under essentially undrained conditions, was measured by SPT and later determined by back-analysis.

**Fig. 14.** Distribution of vertical effective stress $\sigma'_{vo}$ for coefficient of permeability of 0.02 m/day over undrained weak layer in first stage.

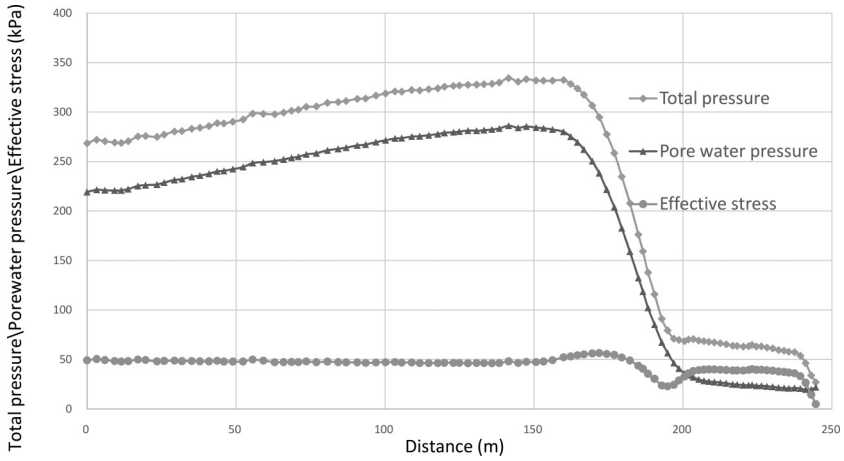


### Geological structure and drainage boundary

Based on the above, the current field in situ testing data gave a reasonable indication of the location, thickness, distribution, and characteristics of the lower weak clay layer in addition to groundwater characteristics. The profile (Fig. 4) was characterized by the lower thin weak clay, confined between a relatively stiff and impermeable clay above and claystone below. The thin weak clay was effectively undrained because of the long lateral drainage paths and low permeability. It was concluded that the seams may become the seat of high excess pore-water pressure during continuous construction, and behave as an essentially undrained condition.

### Failure mechanism

Field investigation of the failure mechanism passing through the waste dump, upper stiff clay, and lower weak clay containing high pore pressure is known as "failure by spreading", as shown in Fig. 4 and described elsewhere in numerous publications (e.g., Cooling and Golder 1942; Varnes 1978; Terzaghi et al. 1996, p. 383; Hungr et al. 2014). A schematic of the pore-water pressure conditions in the lower weak clay is indicated by the dashed line in Fig. 4. The difference between the excess pore-water pressure and the total weight of the overlying soil and waste is lowest near the toe of the slope where the shear strength of the weak clay seam may be close to zero, with resistance to spreading offered only by the passive resistance of the earth located beyond the sliding surface. When this pressure was exceeded, the outer parts of the waste dump moved away from their original positions, resulting in a trough-like depression, as indicated in Figs. 3 and 4.

## Back-analysis of slope stability

Back-analysis of the slope was performed using the strength reduction FE method (e.g., Griffiths and Lane 1999) corresponding to two idealized geometries: (*i*) when the first-level bench reached 16.7 m high and (*ii*) at failure state.

The slope stability analyses made use of the FE programs introduced by Smith and Griffiths (2004) and made use of the "shear strength reduction technique" (Zienkiewicz et al. 1975) to estimate the FoS. Prior to the analysis of slope stability, SIGMA/W was adopted to estimate the distribution of the excess pore-water pressure and vertical effective stress over the lower weak clay layer caused by continuous construction. The procedure of the back-analysis was as follows:

1. Analyze the initial soil stress before the fill loads are applied, using SIGMA/W.
2. Estimate the distribution of the excess pore-water pressure laterally over the lower weak clay layer when the first-level bench reaches 16.7 m using SIGMA/W. The value of $S_u/\sigma'_{vo}$ (assumed constant) is then used to estimate the undrained strength $S_u$ to be used in the first stage of back-analysis.
3. Similar to 2 above, but the value of $S_r/\sigma'_{vo}$ (assumed constant) is then used to estimate the undrained residual strength $S_r$ to be used in the back-analysis corresponding to the failure state.

The FE model was established based on the geological structure and drainage boundaries as shown in Fig. 4. Four types of materials were considered, from top to bottom: the waste dump, upper stiff clay, lower weak clay, and bedrock. The displacement boundary conditions were given as vertical rollers on the left boundary and the lower part of the right boundary and full fixity at the base. To simulate the free surface at the East River bank, the upper part of the right boundary was not constrained. The analysis assumed plane strain conditions and an elastic, perfectly plastic (Mohr–Coulomb) stress–strain rule. Eight-node quadrilaterals were used throughout.

### Determination of engineering properties

According to the categorization scheme of Simmons and McManus (1995), the stripping materials were thought to be dominated by fine-grained, variable plasticity soils. The internal friction angle and cohesion of the waste materials under undrained conditions from these categorization schemes, in combination with empirical values from similar sites and back-analyses described later in this paper, are shown in Table 3.

The undrained peak shear strengths of the upper stiff clay and the bedrock composed of claystone and mudstone are shown in Table 3, which all came from Table 7, giving estimations of the shear strength of the claystone and mudstone below the lower weak clay layer.

After the shear strength of the waste materials, upper stiff clay, and bedrock composed of claystone and mudstone were assessed, the undrained strength of the lower weak clay layer was obtained by back-analyses shown in Table 3.

The Young's modulus and Poisson's ratio for all materials were determined from similar engineering property values (Rowe 2001) although a small number of uniaxial compression tests were performed for the claystone and mudstone. The dilation angle was set to zero.

### Excess pore-water pressure and effective stress analysis

The analyses using SIGMA/W occurred in three stages, and were also based on the geological structure and drainage boundaries as shown in Fig. 4. In the first stage before the fill loads were applied, the initial soil stress conditions were set up based on self-weight with initial pore-water pressure conditions defined by the initial

**Fig. 15.** Back analysis at the end of the first-level bench by finite elements: (*a*) FE mesh; (*b*) displacement vectors (units in metres). [Colour online.]

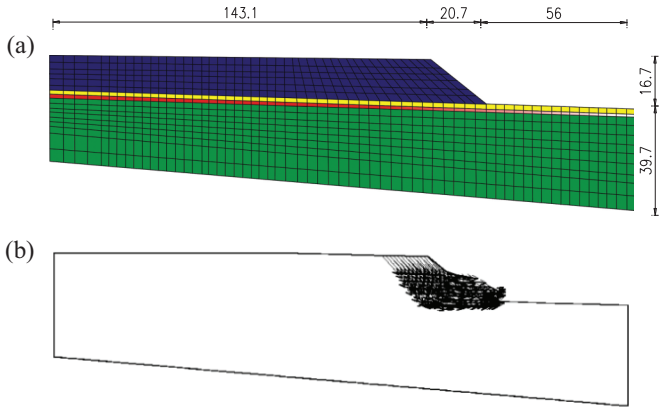


**Fig. 16.** Presence of a crack on the first-level bench during the investigation in 2012. [Colour online.]

water table in the surface residual clay (Fig. 12). In the subsequent two loading stages corresponding to the two stages for the back-analyses of stability, the distribution of the excess pore-water pressure and vertical effective stress were estimated over the lower weak clay using coupled stress – pore pressure analysis, which includes a function able to separate total stress increments into effective stress and pore-water pressure increments. When a linear–elastic model was selected for all materials, which is the most straightforward way of estimating these stress changes (Duncan and Wright 2005, p. 180), results shown in Fig. 13 possessed strong regularity. At this time the material properties of the waste, upper stiff clay, and bedrock, including unit weight, Young's modulus, and Poisson's ratio, were specified for total stress parameters for undrained soils, and the material category of "Effective Parameters w/PWP Change" were assigned for the lower weak clay, in which the coefficient of permeability, volumetric water content function, and hydraulic conductivity function were defined as well as unit weight, effective Young's modulus, and Poisson's ratio (GEO-SLOPE 2008). The volumetric water content function and hydraulic conductivity function for the lower weak clay were simplified to constants according to the given void ratio and permeability values.

From the SIGMA/W analyses, it was noted that the coefficient of permeability of the weak layer had an important influence on the excess pore-water pressure and effective stress. Coefficients of

**Fig. 17.** Comparison of failure modes induced by the different strength ratios $S_r/\sigma'_{vo}$: (*a*) $S_r/\sigma'_{vo} = 0.22$; (*b*) $S_r/\sigma'_{vo} = 0.24$; (*c*) $S_r/\sigma'_{vo} = 0.26$; (*d*) $S_r/\sigma'_{vo} = 0.50$; (*e*) $S_r/\sigma'_{vo} = 0.70$ (units in metres).

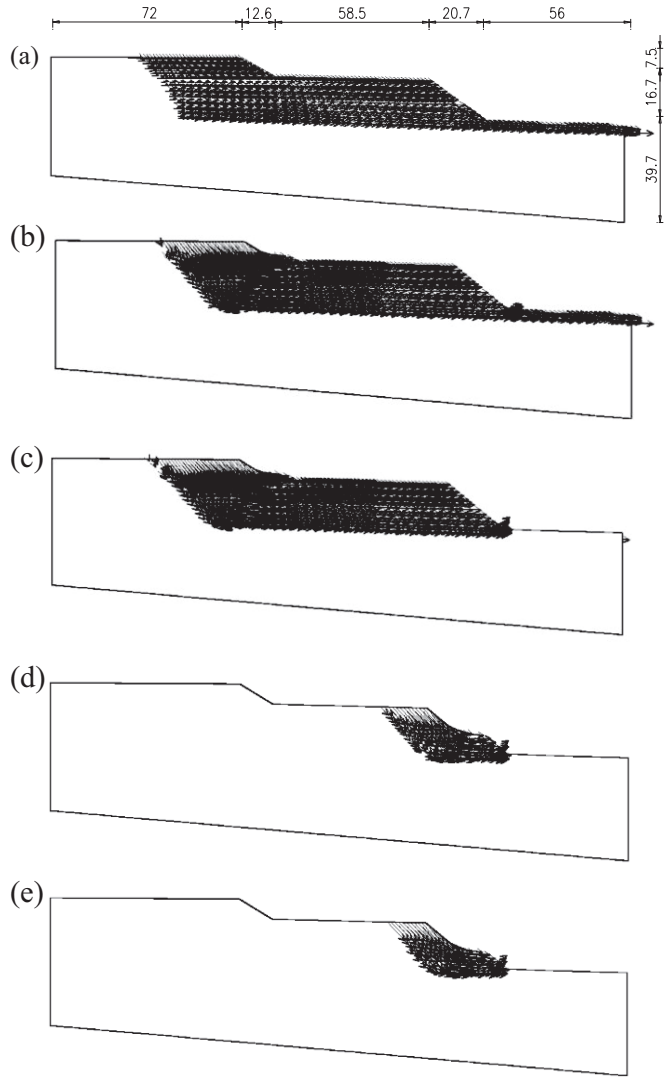


**Table 8.** FOS from different values of $s_r/\sigma'_{vo}$.

| $s_r/\sigma'_{vo}$ | FOS |
|---|---|
| 0.20 | 0.56 |
| 0.22 | 0.61 |
| 0.24 | 0.67 |
| 0.26 | 0.70 |
| 0.50 | 0.89 |
| 0.70 | 0.98 |

permeability of 0.002, 0.02, and 0.2 m/day were assigned in the calculations of vertical effective stress at the time of failure. A comparison of results for the three different parameters is shown in Fig. 13. It is noted that regularity of the three curves is the same although fluctuations in the size have a large difference. Significant fluctuations arose near the toe of the first and second level benches. Outside the toe of the first level bench the effective stress fell significantly and appeared to be negative when the coefficient of permeability was 0.2 m/day, which is unrealistic. Near the toe of the second level bench the variability of effective stress was similar to the first level bench, but smaller. In other parts, the differ-

**Fig. 18.** Distribution of tvertical effective stress $\sigma'_{vo}$ using the coefficient of permeability of 0.02 m/day over undrained weak layer in second stage.

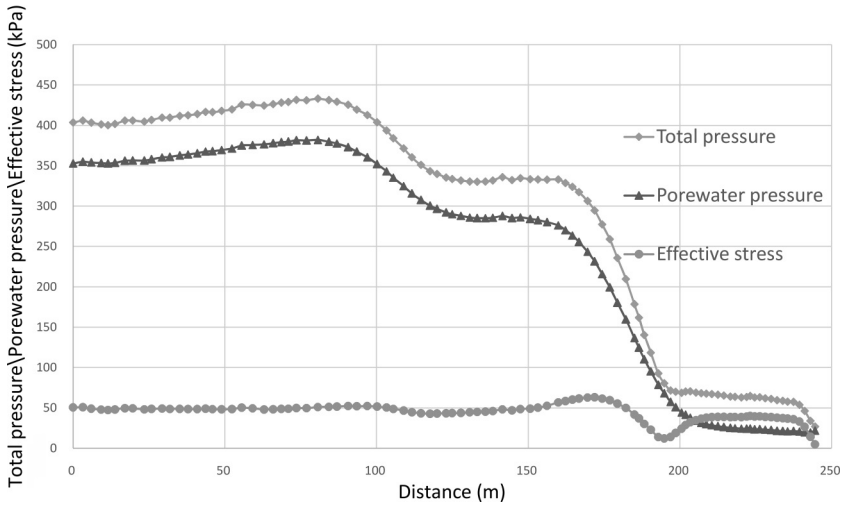


**Fig. 19.** Failure mechanism simulation and stability analysis by finite elements: (*a*) FE mesh; (*b*) displacement vectors (units in metres). [Colour online.]

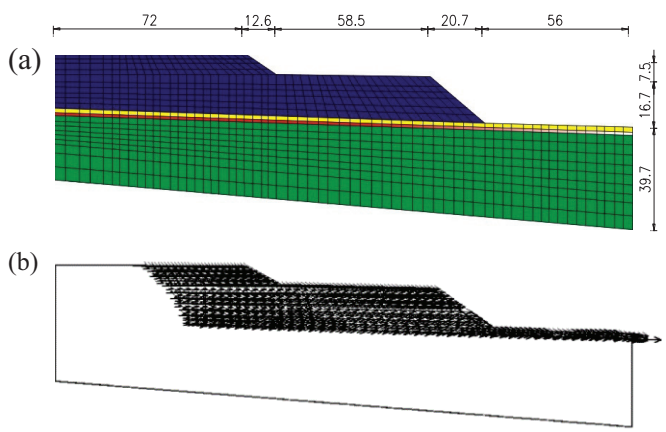


ence between results given by the three different permeabilities was not very significant. According to the extensive investigations summarized in table 14.1 in Terzaghi et al. (1996), the coefficient of permeability for "impervious" soils modified by effects of vegetation and weathering is in the range of $10^{-5}$~$10^{-9}$ m/s, which covers the lower weak clay. Meanwhile, based on the above comparison, a permeability of 0.02 m/day, namely $2.3\times10^{-7}$ m/s, was considered the most realistic for the present study (Table 3).

The distributions of vertical effective stress in the first and second stages were used to obtain the undrained strength (Figs. 14 and 15). The undrained peak strength, $S_u$, and the undrained residual strength, $S_r$, were normalized with respect to the vertical effective stress, $\sigma'_{vo}$, prior to failure. This normalization was performed to evaluate the strength ratio, $S_u/\sigma'_{vo}$, for the first stage, to make the FOS equal to unity and to obtain the strength ratio, $S_r/\sigma'_{vo}$, for the failure state.

### First stage back-analysis of stability

The first stage analysis was done as a back-analysis due to the presence of a crack on the first level bench during the investigation (Fig. 16). When the FOS was equal to unity, the undrained peak strength ratio reached 0.8, indicating a distribution of the vertical effective stress, $\sigma'_{vo}$, over the undrained weak layer shown in Fig. 14. From this, the undrained peak strength values could be estimated and assigned to the corresponding elements of the lower weak clay layer. Figure 15 shows that deformation occurred within the stripping material and then along the weak layer. The first stage back-analysis led to an FOS value of unity, which is clearly an underestimation, as a full failure mechanism did not develop at this stage. The reasons for this are thought to be due to (*i*) the rate of strain-softening in the clay, which may be less than initially assumed, and (*ii*) excess pore-water pressure dissipation and redistribution.

### Failure state back-analysis of stability

When the second level bench reached approximately 7.5 m, a significant failure by spreading occurred. The same parameter values as given in Table 3 were used except for the lower weak clay, which was assigned residual strengths to all the elements.

The sensitivity of the failure mechanism to different values of the ratio $S_r/\sigma'_{vo}$ was investigated as shown in Fig. 17 and Table 8. It was found that the mechanism most similar to that observed in the field (Fig. 5) was obtained when $S_r/\sigma'_{vo} = 0.22$. In addition, it was noted that when $S_r/\sigma'_{vo} = 0.50$ and 0.70, the failure mechanisms were similar to those obtained in the first stage back-analysis, before subsequent loading and further pore pressures were generated.

A further review of the failure state analysis involved reducing the strength of the weak layer from peak to residual in the simulation (Figs. 18 and 19), which led to the FOS of the slope decreasing to 0.61. Figure 20 shows that there were larger fluctuations of effective stress at the time of failure with the increase of loading than in the first stage. The difference between the excess pore-water pressure and the weight of the overlying soil and waste is lowest near the toe of the slope, where the shearing resistance of the lower weak clay may be reduced to near zero. With excess pore pressure dissipation during and after failure, the strength of the weak layer increased with increasing effective stresses, and the FOS of the dump slope returned to values of at least unity.

## Conclusions

The paper has described a case history of a dump slope failure at the Maura Enim Mine in Indonesia, which was induced by excess pore-water pressures generated in a previously undiscovered lower weak clay layer by dumping of waste material. The continuous weak layer existed below the residual clay at about 1.2~4.0 m below ground level, and had a thickness varying in the range of 0.5~1.9 m. The weak layer was relatively permeable (compared with the over- and underlying strata) and could be considered an aquitard, confined between two aquicludes of stiff clay above and stiff claystone below.

**Fig. 20.** Comparison of distribution of vertical effective stress $\sigma'_{vo}$ using coefficient of permeability of 0.02 m/day over undrained weak layer in two stages.

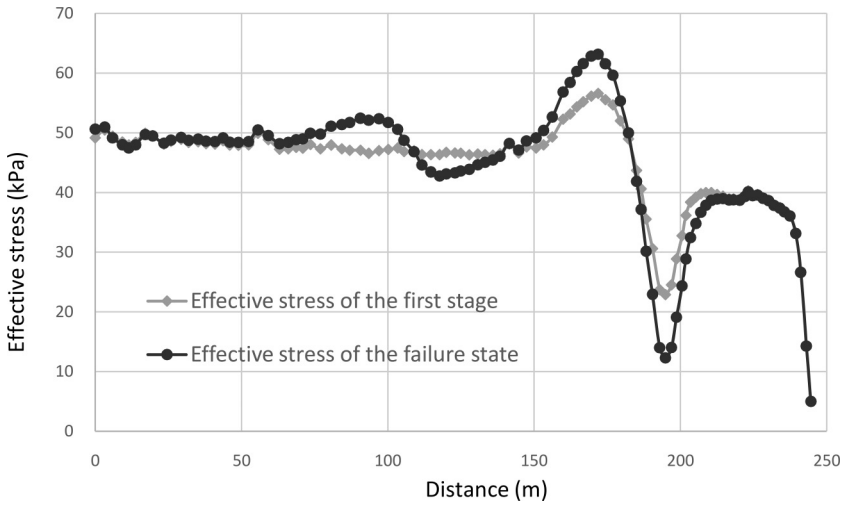


Based on coupled stress – pore pressure analysis to get the distributions of the excess pore-water pressure and vertical effective stress, $\sigma'_{vo}$, the undrained strength ratio led to undrained strength values for the weak layer. When using residual strengths for the weak clay, the FE analysis of the slope led to FOS values significantly below unity. Finite element analyses indicated deformations at failure very similar to those actually observed on site, however, with translational "failure by spreading" towards the river. Failure was most likely initiated at the toe where the vertical effective stress, $\sigma'_{vo}$, was lowest.

From the investigation of the waste dump, the paper has indicated that in a multi-layered slope, the different values of shear strength in the relevant strata can have a very significant effect on the failure mechanism and the FOS. In a back-analysis of such a complex system, the estimation of appropriate soil parameters and excess pore-water pressures presents a significant challenge. There is no doubt, however, that the generation of high pore-water pressures due to dumping in this case was a primary cause of failure.

Lessons to be learned from this case history include primarily the need for a thorough site investigation and laboratory testing program to identify any weak layers ahead of construction. Other remedies in hindsight, especially when dealing with low-permeability strata, might be to include vertical drains to accelerate the process of consolidation, a slower rate of waste dumping or a design involving flatter slopes. In all cases, however, periodic measurement of pore-water pressures and deformation measurements using inclinometers during construction would greatly help to anticipate any impending stability problems.

## Acknowledgement

The first author wishes to thank China Shenhua Group Cor. PT.GH EMM Indonesia for their cooperation and permission to publish this study.

## References

ASTM. 2011*a*. Standard test method for standard penetration test (SPT) and split-barrel sampling of soils. ASTM standard D1586-11. ASTM International, West Conshohocken, Pa.

ASTM. 2011*b*. Standard practice for classification of soils for engineering purposes (Unified Soil Classification System). ASTM standard D2487-11. ASTM International, West Conshohocken, Pa.

Cooling, L.F., and Golder, H.Q. 1942. Correspondence: The analysis of the failure of an earth dam during construction. Journal of the Institution of Civil Engineers, London, **20**(1): 38–55; Discussions, Supplement to No. 8, pp. 289–304.

Dawson, R.F., Morgenstern, N.R., and Stokes, A.W. 1998. Liquefaction flowslides in Rocky Mountain coal mine waste dumps. Canadian Geotechnical Journal, **35**(2): 328–343. doi:10.1139/t98-009.

Duncan, J.M. and Wright, S.G. 2005. Soil strength and slope stability. John Wiley and Sons, Inc. p. 180.

GEO-SLOPE. 2008. Stress-deformation modeling with SIGMA/W 2007.

Griffiths, D.V., and Lane, P.A. 1999. Slope stability analysis by finite elements. Géotechnique, **49**(3): 387–403. doi:10.1680/geot.1999.49.3.387.

Hungr, O., Leroueil, S., and Picarelli, L. 2014. The Varnes classification of landslide types, an update. Landslides, **11**: 167–194. doi:10.1007/s10346-013-0436-y.

Jiao, J.J., Wang, X.S., and Nandy, S. 2005. Confined groundwater zone and slope instability in weathered igneous rocks in Hong Kong. Engineering Geology, **80**: 71–92. doi:10.1016/j.enggeo.2005.04.002.

Ladd, C.C. 1991. Stability evaluation during staged construction. Journal of Geotechnical and Geoenvironmental Engineering, **117**(4): 540–615.

Ministry of Construction of the People's Republic of China. 2009. Code for investigation of geotechnical engineering (GB50021-2001, 2009 edition). National Standard of the People's Republic of China. China Architecture and Building Press, Beijing.

Morgenstern, N.R., and Price, V.E. 1965. The analysis of the stability of general slip surfaces. Géotechnique, **15**(1): 79–93. doi:10.1680/geot.1965.15.1.79.

NSDI. 2009. Geological exploration report of open pit mine of Muara Enim coal-fired power project. Northeast Coalfield Geological Bureau Survey and Design Institute, South Sumatra, Indonesia.

Okagbue, C.O. 1986. An investigation of landslide problems in spoil piles in a strip coal mining area, West Virginia (U.S.A.). Engineering Geology, **22**: 317–333.

PCUT. 2011. Geological survey and stability evaluation of slope of open pit mine of Muara Enim coal-fired power project. Project Group of Chengdu University of Technology, Guohua Indonesia.

Richards, B.G., Coulthard, M.A., and Toh, C.T. 1981. Analysis of slope stability at Goonyella Mine. Canadian Geotechnical Journal, **18**: 179–194. doi:10.1139/t81-023.

Rowe, R.K. (*Editor*). 2001. Geotechnical and geoenvironmental engineering handbook. Springer Science+Business Media, LLC.

Simmons, J.V., and McManus, D.A. 1995. Material categorisation for open pit mining geomechanics. *In* Proceedngs, Bowen Basin Symposium 1995. *Edited by* I.L. Folling, J.W. Beeston, and L.H. Hamilton. Geological Society of Australia, Brisbane.

Smith, I.M., and Griffiths, D.V. 2004. Programming the finite element method. 4rth ed. Chichester: Wiley. doi:10.1002/9781119189237.

Steiakakis, E., Kavouridis, K., and Monopolis, D. Large scale failure of the external waste dump at the "South Field" lignite mine, Northern Greece. Engineering Geology, **104**: 269–279.

SYDRI. 2009*a*. The feasibility study report of Muara Enim open pit Mine. Shenyang Design and Research Institute of Sino Coal International Engineering Group, Indonesia.

SYDRI. 2009*b*. The preliminary design report of Muara Enim open pit Mine. Shenyang Design and Research Institute of Sino Coal International Engineering Group, Indonesia.

Terzaghi, K., Peck, R.B., and Mesri, G. 1996. Soil mechanics in engineering practice, third ed. John Wiley and Sons, Inc., New York, p. 383.

Ulusay, R., Arikan, F., Yoleri, M.F., and Caglan, D. 1995. Engineering geological characterization of coal mine waste material and an evaluation in the context of back-analysis of spoil pile instabilities in a strip mine, SW Turkey. Engineering Geology, **40**: 77–101. doi:10.1016/0013-7952(95)00042-9.

Varnes, D.J. 1978. Slope movement types and processes. *In* Lanslides, analysis and control, special report 176: Transportation research board. *Edited by* R.L. Schuster and R.J. Krizek National Academy of Sciences, Washington, D.C. pp. 11–33.

Zienkiewicz, O.C., Humpheson, C., and Lewis, R.W. 1975. Associated and non-associated viscoplasticity and plasticity in soil mechanics. Géotechnique, **25**: 671–689. doi:10.1680/geot.1975.25.4.671.

## List of symbols

| | |
|---|---|
| $c$, $c'$ | total, effective cohesion |
| $c_u$ | undrained shear strength |
| CF | correction factor |
| COV | coefficient of variation |
| $E$ | undrained Young's modulus |
| $e$ | void ratio |
| FOS | factor of safety |
| $G_s$ | specific gravity |
| $I_p$ | plasticity index |
| $N$ | measured blow count of SPT |
| $N_{60}$ | corrected blow count of SPT with hammer drop height adjusted to provide 60% energy |
| $N_{63.5}$ | corrected blow count of DCPT with drop weight of 63.5 kg and drop distance of 76 cm |
| $N'_{63.5}$ | measured blow count of DCPT with drop weight of 63.5 kg and drop distance of 76 cm |
| $q_u$ | unconfined compressive strength |
| $w$ | water content |
| $w_l$ | liquid limit |
| $w_p$ | plastic limit |
| $S_r$ | degree of saturation |
| $S_r$ | undrained residual strength |
| $S_u$ | undrained peak strength |
| $S_r/\sigma'_{vo}$ | undrained residual strength ratio |
| $S_u/\sigma'_{vo}$ | undrained peak strength ratio |
| SD | standard deviation |
| SV | standard value |
| $\nu$ | undrained Poisson's ratio |
| $\alpha_1$ | correction coefficient of DCPT |
| $\gamma$ | total unit weight |
| $\gamma_d$ | dry unit weight |
| $\sigma$ | normal stress |
| $\sigma'_{vo}$ | effective vertical stress |
| $\tau$ | shear stress |
| $\phi$, $\phi'$ | total, effective friction angle |